JOURNAL OF APPLIED PHYSICS **108**, 124302 (2010)

Carrier dynamics in β-Ga_2O_3 nanowires

Andreas Othonos,[1,a] Matthew Zervos,[2] and Constantinos Christofides[3]
[1]*Department of Physics, Research Center of Ultrafast Science, University of Cyprus, P.O. Box 20537, Nicosia 1678, Cyprus*
[2]*Department of Mechanical Engineering, Nanostructured Materials and Devices Laboratory, University of Cyprus, P.O. Box 20537, Nicosia 1678, Cyprus*
[3]*Department of Physics, Photonics and Optoelectronics Research Laboratory, University of Cyprus, P.O. Box 20537, Nicosia 1678, Cyprus*

(Received 26 July 2010; accepted 25 October 2010; published online 17 December 2010)

Carrier dynamics have been investigated in β-Ga_2O_3 nanowires (NWs) grown by the vapor-liquid-solid mechanism, using ultrashort transient absorption spectroscopy in conjunction with time-correlating single photon counting photoluminescence. UV femtosecond pulse excitation has been utilized to generate nonequilibrium carrier distributions near the band edge of the NWs and nondegenerate pump-probe techniques have been employed to follow carrier relaxation through the defect related states located within the band gap of the NW semiconductor. Relaxation of the photogenerated carriers through these states appears to be biexponential with a fast component on the order of 3–5 ps and the slower component around 40–90 ps depending on the states being probed. Transient absorption intensity measurements reveal that recombination mechanisms such as Auger and bimolecular become contributing factors to the relaxation dynamics for absorbed fluences larger than 90 $\mu J/cm^2$. In the low fluence regime, time-correlated single photon counting photoluminescence measurements revealed a nonradiative relaxation mechanism with time constants ranging from 0.6–1 ns and a radiative relaxation with a time constant of approximately 4 ns. © *2010 American Institute of Physics*. [doi:10.1063/1.3520589]

I. INTRODUCTION

Semiconductor, metal-oxide (MO) nanowires (NWs) have been investigated widely over the past decade as building blocks for the fabrication of novel electronic and optoelectronic nanoscale devices but also sensors and third generation solar cells due to their properties arising from their small size and high surface-to-volume ratio. Among the MO NWs, β-Ga_2O_3 with monoclinic structure has one of the largest band gaps of ≈4.9 eV (Ref. 1) which emits over a wide range of wavelengths from the infrared to ultraviolet.[2–4] This property makes it a candidate for gas sensing,[5] catalytic,[6] and optoelectronic devices applications.[7] The study of the synthesis and optical properties of one-dimensional β-Ga_2O_3 nanostructures has attracted considerable interest due to their potential application in nanodevices. Thus, far nanorods, nanobelts, nanoribbons, and nanotubes[8–20] have been grown using the vapor liquid solid (VLS) mechanism,[8–11] direct thermal evaporation using Ga_2O_3, Ga, or GaN powders[12–15] or by using microwave plasma reactions.[16] The β-Ga_2O_3 NWs have n-type conductivity attributed to native oxygen vacancies while many studies have shown that β-Ga_2O_3 NWs exhibit highly intense, blue photoluminescence (PL) with emission between 400–500 nm. In order to complement our earlier work on SnO_2,[21] In_2O_3,[22] NW and corresponding nitrides, i.e., GaN,[23] InN,[24] and Sn_3N_4,[25] we have carried out a detailed investigation into the ultrafast, carrier relaxation mechanisms of photogenerated carriers in β-Ga_2O_3 NWs. This information may be used to improve our fundamental understanding of their optical properties which is important for the realization of nanoscale devices.[26–28] It should be emphasized that time resolved, pump-probe measurements in β-Ga_2O_3 NWs are not trivial mainly due to the difficulties associated with the excitation of carriers into the conduction band due to its large band gap of 4.9 eV. In this work, we have investigated carrier dynamics in β-Ga_2O_3 NWs in order to obtain a detailed understanding of the various relaxation mechanisms and the influence of trap states using transient femtosecond absorption spectroscopy in conjunction with time-correlated single photon counting (TCSPC) PL. We find that following above-band gap excitation carrier relaxation toward equilibrium occurs through a number of states located within the band gap of the β-Ga_2O_3 NWs, related to defects such as oxygen vacancies and surface states. Transient absorption measurements reveal a double exponential relaxation (fast and slow components) for the photogenerated carriers. The fast relaxation (3–5 ps) is associated with carrier redistribution within the probed energy state region, whereas the slower component (40–90 ps) is attributed to relaxation of the photogenerated carriers into energy states further from the probed region, possibly related to surface states. There does not appear to be any noticeable interaction between the carriers generated at the surface plasmon resonance in the Au nanoparticle and the carriers in the β-Ga_2O_3 NWs on a picosecond time scale. TCSPC measurements reveal radiative and nonradiative relaxation mechanisms on a nanosecond timescale for the photogenerated carriers.

II. RESULTS AND DISCUSSION

Gallium oxide, β-Ga_2O_3 NWs were grown using an atmospheric pressure chemical vapor deposition reactor which

[a]Electronic mail: othonos@ucy.ac.cy.

 © 2010 American Institute of Physics

Downloaded 23 Dec 2010 to 194.42.7.185. Redistribution subject to AIP license or copyright; see http://jap.aip.org/about/rights_and_permissions

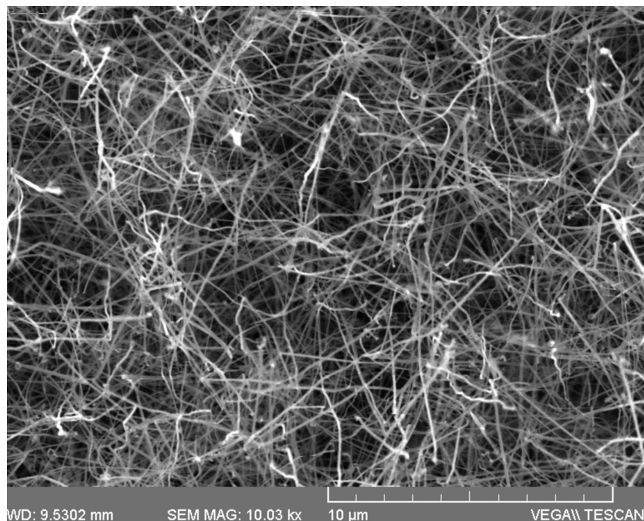

FIG. 1. Typical SEM image of Ga_2O_3 NWs obtained at T_G=900 °C under 100 SCCM's Ar on 0.7 nm Au/Si(001).

consists of four mass flow controllers and a 1″ horizontal quartz tube (QT) furnace, capable of reaching a maximum temperature of 1100 °C. Upon installation, each 1″ QT was always heated to 900 °C at 30 °C/min and maintained at 900 °C for 15 min under a constant flow of 100 standard cubic centimeters per minute (SCCMs) of Ar after which it was allowed to cool down to room temperature (RT). For the growth of β-Ga_2O_3 NWs, 0.1–0.5 g of solid Ga fragments (Aldrich, 99.99%) stored below its melting point of 30 °C were cut, weighed, and loaded in a quartz boat while square pieces of n^+ Si(001) ≈7 mm×7 mm or quartz coated with 0.5 nm's of Au, were loaded at various distances from the Ga (the Si substrate samples were used in the PL measurements whereas the quartz substrate in the transient absorption measurements). The Au layer was deposited via sputtering using an Ar plasma under a pressure of $\approx 10^{-2}$ mbar. The boat was always loaded into the reactor and was positioned directly above the thermocouple used to measure the heater temperature (T_H) at the center of the 1″ QT. After closing the reactor Ar was introduced at a flow rate of 500 SCCM's for 10 min. Then the temperature was ramped to the desired growth temperature under a reduced flow of 100 SCCM Ar using a ramp rate of 30 °C/min. Upon reaching the growth temperature (T_G) the Ar flow was maintained at 100 SCCMs for 1 h after which the tube was allowed to cool down using the same gas flows during growth. The sample was removed only when the temperature was lower than 100 °C. The morphology of all as-grown β-Ga_2O_3 NWs were examined with a TESCAN scanning electron microscope (SEM) while their crystal structure and the phase purity were investigated using a SHIMADZU, XRD-6000, x-ray diffractometer with a Cu $K\alpha$ source by performing a scan of θ-2θ in the range between 10° and 80°.

A typical SEM image of the β-Ga_2O_3 NWs obtained is shown in Fig. 1. The diameters of the β-Ga_2O_3 NWs are ≈50 nm and their lengths ≥10 μm. It should be pointed out that a high yield of β-Ga_2O_3 NWs was obtained when the distance between the Ga and Au/Si(001) was <5 mm and the mass of Ga fragments used in the reaction varied

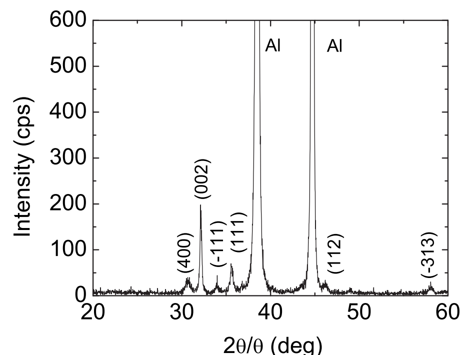

FIG. 2. XRD corresponding to monoclinic β-Ga_2O_3 with lattice constants a=12.23 Å, b=3.04 Å, c=5.80 Å, and β=103.7°.

between 0.1–0.3 g which led to a white-blue like deposit. In addition the distribution of β-Ga_2O_3 NWs was very uniform across the entire surface of the 7 mm^2 sample. Note that the growth of the β-Ga_2O_3 NWs is attributed to the reaction of Ga with residual O_2 in the reactor similar to the growth of other semiconductor oxide NWs such as SnO_2 (Ref. 21) and In_2O_3.[22] A high yield-uniform distribution of β-Ga_2O_3 NWs was easily and reproducibly obtained on 0.7 nm Au/Si(001) while one can also observe Au NPs on their ends confirming that they grow via the VLS mechanism. The β-Ga_2O_3 NWs exhibited pronounced peaks in the XRD as shown in Fig. 2 corresponding to monoclinic β-Ga_2O_3 with lattice constants a=12.23 Å, b=3.04 Å, c=5.80 Å, and β=103.7°.[29]

Figure 3 below shows typical PL obtained from the β-Ga_2O_3 NWs when excited with 255 nm. The PL is broad covering a spectral range from 290 to 800 nm with a peak around 520 nm. This is a typical PL spectrum obtained from β-Ga_2O_3, where the broad emission is associated with states due to O, Ga, and Ga–O vacancies[2,30] which are located within the band gap.[31] It is expected that O vacancies and Ga–O vacancy pairs are present in the β-Ga_2O_3 considered here, given that the synthesis of the NWs was carried out at high temperature in an oxygen-deficient environment thus

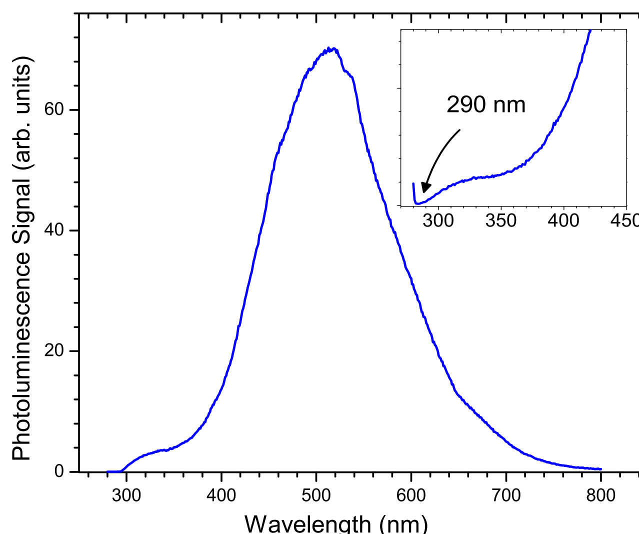

FIG. 3. (Color online) RT PL spectrum of β-Ga_2O_3 NWs excited with a light source at 255 nm. The inset figure show the smallest PL emission wavelength which occurs at 290 nm.

Downloaded 23 Dec 2010 to 194.42.7.185. Redistribution subject to AIP license or copyright; see http://jap.aip.org/about/rights_and_permissions

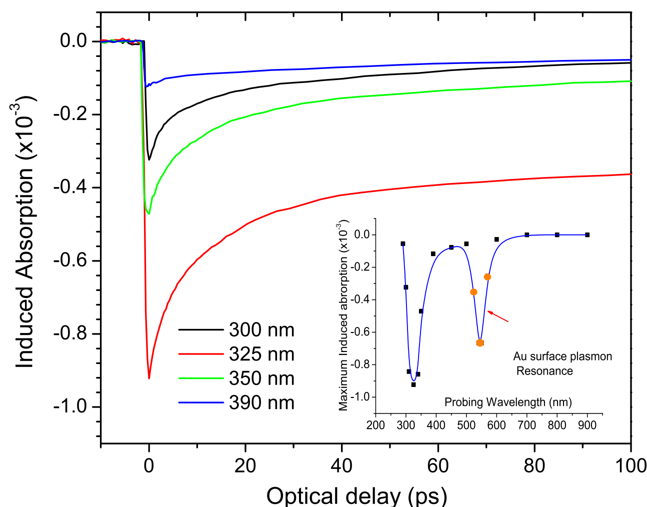

FIG. 4. (Color online) Transient absorption traces of the Ga_2O_3 NWs at different probing wavelengths with excitation at $\lambda = 252$ nm. The inset shows the maximum induced absorption as a function of the probing wavelength.

resulting to the observed broad defect PL. Here, we should point out that PL measurements carried out without the cut-off filters provided an upper bound of 290 nm in the emission spectrum as seen in the inset of Fig. 3.

To investigate the dynamics of this wide-band gap oxide on a femtosecond timescale we used an ultrafast laser amplifier. This amplifier is based on a self-mode lock Ti:sapphire oscillator producing a train of pulses at 76 MHz centered at 796 nm (1.55 eV) with a full-width-half-maximum of 45 fs. These pulses were then amplified by approximately 10^6 times using a chirp pulse amplifier at the expense of reducing the repetition rate at 1 kHz. The amplified pulses where then used to generated various wavelengths of light via optical parametric amplification and white light generation. These ultrafast pulses are then used in a typical pump-probe noncollinear configuration to measure time resolved transmission and reflection (transient absorption) in the β-Ga_2O_3 NWs using lock-in amplifier phase detection.

In the transient absorption measurements, UV ultrafast pulses at 252 nm (4.92 eV) were used to excite the β-Ga_2O_3 NWs, whereas much weaker pulses in the spectral range between UV to IR were used to probe the various energy states in the NWs. Figure 4 show transient induced absorption measurements obtained at an estimated absorbed fluence of approximately 75 $\mu J/cm^2$ which corresponds to a carrier density of approximately 1.2×10^{19} cm^{-3}. Clearly evident in these measurements is the pulse width limited, sharp drop in the induced absorption followed by a recovery toward equilibrium over a time scale of 100 ps.

These observed changes in absorption are associated with the excitation of the β-Ga_2O_3 NWs by photons whose energy is larger than the band gap resulting in the generation of nonequilibrium carriers. These nonequilibrium carriers will redistribute themselves among energy states that are normally unoccupied under equilibrium conditions. The occupation of states, referred to as state filling, following an ultrafast laser pulse will appear as a reduction in the absorption at the energy states being probed. Clearly the observed recovery of this negative absorption change will be a direct measure of the time required by the photogenerated carriers to move out of the occupied states.

The observed negative change in the transient absorption traces (state filling), for probing wavelengths with photon energies smaller than 4.2 eV (295 nm) suggests that energy states are located within the band gap of the β-Ga_2O_3 NWs, in agreement with the observed PL emission. Furthermore, we should point out that the strength of the induced absorption signal depends on the density of states and the number of carriers present at the energy state being probed. Given that the carriers are initially generated in the conduction band and then are distributed among the states within the band gap during energy relaxation, then, to a first approximation, we may assume that the strength of the signal is directly related to the density of states at the probing wavelength. The inset in Fig. 4 depicts this behavior, where a graph of the maximum induced change has been plotted against the probing wavelength. The energy states located within the band gap covering a range between 2 to 4.2 eV (619–295 nm) have two minima the first located at 3.8 eV (326 nm) and the second at 2.30 eV (539 nm) from the valence band. The fist minimum is associated with high density of defect states located within the band gap of the NWs which is in agreement with the observed PL peak at 330 nm in β-Ga_2O_3 NWs by Liang.[9] On the other hand the second minimum corresponds to the surface plasmon resonance band of the Au nanoparticle attached to the end of the NW, required for the formation of β-Ga_2O_3 nanostructures. This plasmon resonance is due to the electron interaction with the electromagnetic field, associated with intraband and interband transitions of conduction electrons between 5*d* and 6*s* orbitals.[32–34] In order to confirm this, we repeated the experiment using only 0.5 nm Au on quartz substrate and observed the same behavior in the region between 520–580 nm. No signal was detected in other spectral regions. To further investigate possible interaction between Au nanoparticle and the β-Ga_2O_3 NWs, time resolved measurements were carried out with ultrafast pulses at 3.1 eV (400 nm) corresponding to excitation below the band edge and compared with those carried out using excitation at 4.9 eV (252 nm). Measurements reveal identical temporal behavior near the surface plasmon resonance band whereas no signal away from the resonance was observed with the 3.1 eV excitation. This identical temporal behavior suggests that there is no noticeable interaction, that is, within the sensitivity of the experiment, between photogenerated carriers in the β-Ga_2O_3 NWs, and those in the Au nanoparticle on a 100 ps timescale. This may not necessarily be true for a longer time scale where possible energy transfer may occur between the two connected nanostructures (although this is expected to be a relatively small effect).

To help the reader obtain a clear picture of the dynamics in β-Ga_2O_3, NWs we have included a schematic band diagram model in Fig. 5 showing the various energy states related to defects and relaxation mechanisms utilized in our interpretation. Following excitation, carriers near the band edge will relax into the defect/vacancy (gap-) states (mechanism "1"). These carriers will then be redistributed among the gap-states via fast nonradiative interaction "2" or slower

Downloaded 23 Dec 2010 to 194.42.7.185. Redistribution subject to AIP license or copyright; see http://jap.aip.org/about/rights_and_permissions

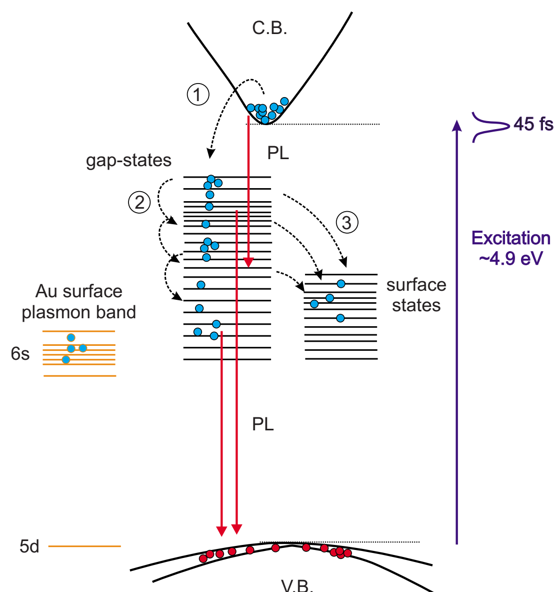

FIG. 5. (Color online) Schematic diagram of a model showing pulse excitation at 4.9 eV and subsequent relaxation of the photoexcited carriers in the Ga_2O_3 NWs. The vertical red arrows indicate the PL emission states. Surface states provide a relaxation path of the photogenerated carriers within the gap-states. The states on the left of the band diagram represent the surface plasmon resonance band of the Au nanoparticles attached to the NWs.

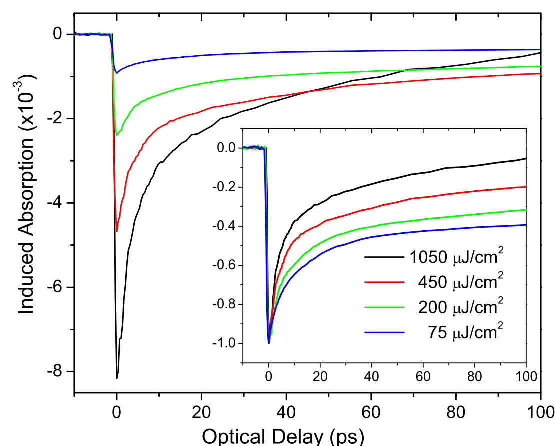

FIG. 6. (Color online) Intensity dependent nondegenerate transient absorption measurements of the Ga_2O_3 NWs with excitation at λ=252 nm. The inset shows the same data normalized for comparison. The values in the legends correspond to the absorbed fluence.

radiative emission. Surface states also play key role in the relaxation of the photogenerated carriers "3." The observed PL which has a broad spectral range between 290–800 nm as shown in Fig. 3 is represented by vertical red arrows and is mainly associated with radiative relaxation of the photogenerated carriers within the band gap due to the various vacancies and defect states. Also shown on the schematic is the surface plasmon absorption band due to the Au nanoparticles attached to the NWs.

Next, the temporal behavior of the transient absorption measurements were analyzed in detail using a multiexponential fit to the data of Fig. 4. The analysis reveals that a minimum requirement of two exponential functions is necessary for a good fit to the data. The time constants obtained from these fits were 3–5 ps (40%–20%), 38–90 ps (46%–60%), and A_0 (13%–36%) as seen in Table I. The fast component (3–5 ps) is associated with the redistribution of the photogenerated carriers around the probing energy states of the NWs ("2" Fig. 5), whereas the longer time constant is most likely associated with the relaxation of the carriers to energy states

TABLE I. Time constants from a double exponential fit of $I(t)=A_0 + A_1 e_1^{-t/\tau} + A_2 e_2^{-t/\tau}$ to the transient absorption data.

λ (nm)	A_0 (%)	n=1 τ_n (ps)	n=1 A_n (%)	n=2 τ_n (ps)	n=2 A_n (%)
300	13	3.2	41	43	46
325	36	5.4	30	38	30
350	20	5.4	40	45	40
390	22	3.9	20	90	58
450	25	4.5	25	85	50

located far from the probing region such as surface states. The observed variation in the lifetime as a function of probing wavelength is most likely associated with the available relaxation, coupling states at the particular probing energy state. The twofold increase in the lifetime as seen for the probing wavelengths of 390 and 450 nm (Table I, n=2) suggests a coupling to different relaxation states, however, this is not well understood due to the complex nature of the defect and surface states in this NW system. Here we should point out that the A_0 constant corresponds to the presence of a significant carrier density on a long time scale in comparison to the 100 ps scale. These carriers are most likely the carriers which contribute to the observed PL.

To investigate further the ultrafast carrier relaxation behavior in the β-Ga_2O_3 NWs, we carried out intensity dependent transient absorption measurements at the key probing wavelengths. Figure 6 shows transient absorption measurements obtained using UV excitation pulses at 252 nm and probing photons at 325 nm. For the purpose of comparison these data were normalized and plotted as seen in the inset of Fig. 6. Clearly evident is the faster recovery with increasing incident photon flux suggesting that mechanisms such as bimolecular and Auger recombination[28,35] play a significant role in the energy relaxation of the photogenerated carriers even for energy states located below the band edge of the semiconductor NWs. Similar measurements were carried out at the plasmon resonance peak and we notice exactly the opposite effect. Namely an increase in the recovery time with increasing incident fluence.[36] This behavior was also confirmed with the 0.5 nm Au film as well as with the excitation of the NW samples with 3.1 eV pulses.[36]

To obtain a better understanding of the dynamics in the NWs on a longer time scale, time resolved PL were carried out using TCSPC. The excitation was carried out using a Ti:sapphire ultrafast amplifier generating 255 nm at a repetition rate of 250 kHz. The spot size of the focused beam was ≈2 mm and generated a carried density which was several orders of magnitude smaller than the carrier density in the Auger regime seen in the transient absorption experiments. A further reduction in the incident intensity using a neutral den-

Downloaded 23 Dec 2010 to 194.42.7.185. Redistribution subject to AIP license or copyright; see http://jap.aip.org/about/rights_and_permissions

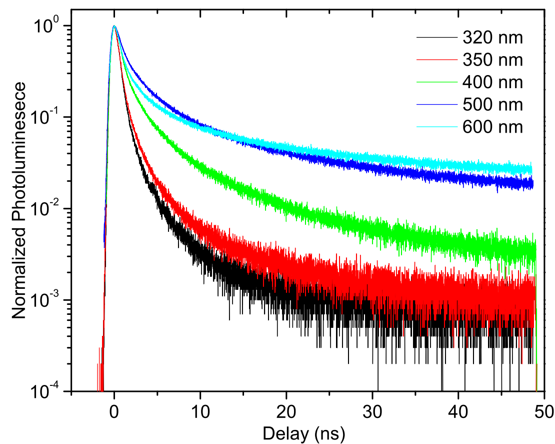

FIG. 7. (Color online) TCSPC PL from Ga_2O_3 NWs excited with ultrafast pulses at 255 nm and probe at 320, 350, 400, 500, and 600 nm.

sity filter in front of the laser source revealed that the time constants were independent of the incident intensity. Figure 7 shows TCSPC data obtained at several emission wavelengths namely at $\lambda=320$, 350, 400, 500, and 600 nm over a time span of 50 ns. Clearly different decays profiles are obtained for the different probing wavelengths.

Analysis of the decay curves reveals that the data profiles are well described by an exponential function of the form $I(t)=A_1 e_1^{-t/\tau}+A_2 e_2^{-t/\tau}+A_3\, e_3^{-t/\tau}$, suggesting a complex energy level structure for the β-Ga_2O_3 NWs. The exponential time constants and their associated strengths are shown in Table II. This multiexponential decay of the PL signal indicates the existence of nonradiative channels available to the probing carriers. Although the measured PL signal comes from a particular energy state, the nonradiative channels available to the photogenerated carriers in these states alter the population thus making the PL decay appear multiexponential.

It is interesting to point out that for the short emission wavelengths the fitting was accomplished using only a double exponential function. Whereas for emission wavelengths around the peak PL it was necessary to use a triexponential function for a good fit to the data. The first time constant in the exponential function is subnanosecond and most likely associated with nonradiative relaxation of the carriers within vacancy and surface related states. The strength of this time constant (A_1) is smaller near the 500 nm emission suggesting that this nonradiative component is less important near the peak of PL as expected thus allowing more carriers to be available for radiative relaxation. The second time constant as seen in Table II is approximately 4 ns and it most likely associated with the PL emission in these NWs. This is further supported from that fact that the strength of this time constant is largest at the peak of the radiative emission in agreement with PL data. The third component observed (in Table II) which is very weak, maybe due to several factors, including additional radiative and nonradiative channels and possibly energy transfer from the Au nanoparticles to the carriers in the NWs. This, however, cannot be clarified further at this time, mainly due to the complex nature of the defects states and the requirement of the Au nanoparticles for the synthesis of this nanostructure material.

TABLE II. Time constants from a triexponential fit of $I(t)=A_1 e_1^{-t/\tau}+A_2 e_2^{-t/\tau}+A_3\, e_3^{-t/\tau}$ to the curves of Fig. 7.

	n=1		n=2		n=3	
λ (nm)	τ_n (ns)	A_n (%)	τ_n (ns)	A_n (%)	τ_n (ns)	A_n (%)
320	0.64	97	4.5	3	⋯	⋯
350	0.67	94	4.0	6	⋯	⋯
400	0.85	80	4.3	18	43.1	2
500	1.01	63	4.2	30	20.2	7
600	0.81	76	4.1	18	23.2	6

III. CONCLUSIONS

We have investigated carrier dynamics of β-Ga_2O_3 NWs using femtosecond transient absorption spectroscopy and TCSPC PL. Following ultrafast pulse excitation near the band edge, energy relaxation of the photogenerated carriers occurs via nonradiative and radiative mechanisms in states located within the band gap of the NWs. Transient absorption measurements reveal a plethora of energy states located between 4.2 to 2.5 eV above the valence band which are associated with vacancies and surface states inherit in the growth of the β-Ga_2O_3 NWs. A plot of the maximum induced absorption as a function of probing wavelength revealed two minima with the larger contributions occurring at 3.8 eV being associated with a high density of defect states in the NWs and the second occurring at 2.3 eV associated with the surface plasmon resonance band of the Au nanoparticle used as the seed for the synthesis of the NWs. The photogerated carriers in these β-Ga_2O_3 NWs follow a decay described by a two exponential relaxation function, with the fast mechanism having a time constant of 3–5 ps and the slower one 40–90 ps, both associated with nonradiative relaxation of the photogenerated carriers within the defect and surface states. Recombination mechanisms such as Auger and bimolecular has a non-negligible contribution for an incident fluence larger than 90 $\mu J/cm^2$. TCSPC measurements provided evidence of the radiative and nonradiative relaxation mechanisms on a nanosecond timescale. Analysis suggested a double exponential function was necessary for a good fit to the data in the UV spectra range whereas a triexponential was necessary for probing wavelengths near the surface plasmon resonance. The fast component was attributed to nonradiative relaxation within the gap-states, whereas the second component (~4 ns) was identified as the radiative relaxation. Finally the third component was attributed to additional radiative channels in the NWs or possible energy transfer from the Au NPs at the surface plasmon resonance thus providing an additional relaxation channel to the carriers at the emission wavelength.

ACKNOWLEDGMENTS

The work in this article was partially supported by the research Program Nos. ERYAN/0506/04, ERYNE/0506/02,

Downloaded 23 Dec 2010 to 194.42.7.185. Redistribution subject to AIP license or copyright; see http://jap.aip.org/about/rights_and_permissions

and BE0308/03 funded by the Cyprus Research Promotion Foundation in Cyprus.

[1]H. H. Tippins, Phys. Rev. **140**, A316 (1965).
[2]L. Binet and D. Gourier, J. Phys. Chem. Solids **59**, 1241 (1998).
[3]Y. P. Song, H. Z. Zhang, C. Lin, Y. W. Zhu, G. H. Li, F. H. Yang, and D. P. Yu, Phys. Rev. B **69**, 075304 (2004).
[4]E. Nogales, B. Mendez, and J. Piqueras, Appl. Phys. Lett. **86**, 113112 (2005).
[5]M. Fleischer and H. Meixner, Sens. Actuators B **4**, 437 (1991).
[6]A. L. Petre, A. Auroux, P. Gelin, M. Caldararu, and N. I. Ionescu, Thermochim. Acta **379**, 177 (2001).
[7]T. Miyata, T. Nakatani, and T. Minami, J. Lumin. **87–89**, 1183 (2000).
[8]Y. Huang, S. Yue, Z. Wang, Q. Wang, C. Shi, Z. Xu, X. D. Bai, C. Tang, and C. Gu, J. Phys. Chem. B **110**, 796 (2006).
[9]C. H. Liang, G. W. Meng, G. Z. Wang, Y. W. Wang, L. D. Zhang, and S. Y. Zhang, Appl. Phys. Lett. **78**, 3202 (2001).
[10]K.-W. Chang and J.-J. Wu, Adv. Mater. (Weinheim, Ger.) **16**, 545 (2004); J. Mater. Res. **20**, 3397 (2005).
[11]P. Feng, J. Y. Zhang, Q. H. Li, and T. H. Wang, Appl. Phys. Lett. **88**, 153107 (2006).
[12]L. Fu, Y. Liu, P. Hu, K. Xiao, G. Yu, and D. Zhu, Chem. Mater. **15**, 4287 (2003).
[13]H. Z. Zhang, Y. C. Kong, Y. Z. Wang, X. Du, Z. G. Bai, J. J. Wang, D. P. Yu, Y. Ding, Q. L. Hang, and S. Q. Feng, Solid State Commun. **109**, 677 (1999).
[14]Z. R. Dai, Z. W. Pan, and Z. L. Wang, J. Phys. Chem. B **106**, 902 (2002).
[15]J. Zhan, Y. Bando, J. Hu, Y. Li, and D. Golberg, Chem. Mater. **16**, 5158 (2004).
[16]F. Zhu, Z. X. Yang, W. M. Zhou, and Y. F. Zhang, Solid State Commun. **137**, 177 (2006).
[17]S. Sharma and M. K. Sunkara, J. Am. Chem. Soc. **124**, 12288 (2002).
[18]J. Hu, Y. Bando, D. Golberg, and Q. Liu, Angew. Chem. Int. Ed. **42**, 3493 (2003).
[19]J. Zhang, F. Jiang, Y. Yang, and J. Li, J. Phys. Chem. B **109**, 13143 (2005).
[20]Y. Wang, L. Hou, X. Qin, S. Ma, B. Zhang, H. Gou, and F. Gao, J. Phys. Chem. C **111**, 17506 (2007).
[21]A. Othonos, M. Zervos, and D. Tsokkou, Nanoscale Res. Lett. **4**, 828 (2009).
[22]D. Tsokkou, A. Othonos, and M. Zervos, J. Appl. Phys. **106**, 084307 (2009).
[23]D. Tsokkou, A. Othonos, and M. Zervos, J. Appl. Phys. **106**, 054311 (2009).
[24]A. Othonos, M. Zervos, and M. Pervolaraki, Nanoscale Res. Lett. **4**, 122 (2009).
[25]A. Othonos and M. Zervos, J. Appl. Phys. **106**, 114303 (2009).
[26]R. P. Prasankumar, P. C. Upadhya, and A. J. Taylor, Phys. Status Solidi B **246**, 1973 (2009).
[27]P. Parkinson, J. Lloyd-Hughes, Q. Gao, H. H. Tan, C. Jagadish, M. B. Johnston, and L. M. Herz, Nano Lett. **7**, 2162 (2007).
[28]I. Robel, B. A. Bunker, P. V. Kamat, and M. Kuno, Nano Lett. **6**, 1344 (2006).
[29]C. L. Kuo and M. H. Huang, Nanotechnology **19**, 155604 (2008).
[30]T. Harwig and F. Kellendonk, J. Solid State Chem. **24**, 255 (1978).
[31]L. Cao, M. K. Li, Z. Yang, Q. Wei, and W. Zhang, Appl. Phys. A: Mater. Sci. Process. **91**, 415 (2008).
[32]A. Devizis, V. Vaicikauskas, and V. Gulbinas, Appl. Opt. **45**, 2535 (2006).
[33]S. Link, C. Burda, Z. L. Wang, and M. A. El-Sayed, J. Chem. Phys. **111**, 1255 (1999).
[34]T. S. Ahmadi, S. L. Logunov, and M. A. El-Sayed, J. Phys. Chem. **100**, 8053 (1996).
[35]P. C. Upadhya, Q. Li, G. T. Wang, A. J. Fischer, A. J. Taylor, and R. P. Prasankumar, Semicond. Sci. Technol. **25**, 024017 (2010).
[36]J. Hodak, I. Martini, and G. V. Hartland, Chem. Phys. Lett. **284**, 135 (1998).

Downloaded 23 Dec 2010 to 194.42.7.185. Redistribution subject to AIP license or copyright; see http://jap.aip.org/about/rights_and_permissions